UNCONVENTIONAL
RESOURCES TECHNOLOGY CONFERENCE
FUELED BY SPE • AAPG • SEG

URTeC: 415

Marcellus Shale Energy and Environmental Laboratory (MSEEL) Results and Plans: Improved Subsurface Reservoir Characterization and Engineered Completions

Timothy R. Carr*[1], Payam Kavousi Ghahfarokhi[1], BJ Carney[2], Jay Hewitt[3], Robert Vagnetti[4]; 1. West Virginia University, 2. Northeast Natural Energy, 3 Hewitt Energy Strategies, 4. US Department of Energy, National Energy Technology Laboratory.

This paper was prepared for presentation at the Unconventional Resources Technology Conference held in Denver, Colorado, USA, 22-24 July 2019.

Abstract

The Marcellus Shale Energy and Environment Laboratory (MSEEL) involves a multidisciplinary and multi-institutional team of universities companies and government research labs undertaking geologic and geomechanical evaluation, integrated completion and production monitoring, and testing completion approaches. MSEEL consists of two legacy horizontal production wells, two new logged and instrumented horizontal production wells, a cored vertical pilot bore-hole, a microseismic observation well, and surface geophysical and environmental monitoring stations. The extremely large and diverse (multiple terabyte) datasets required a custom software system for analysis and display of fiber-optic distributed acoustic sensing (DAS) and distributed temperature sensing (DTS) data that was subsequently integrated with microseismic data, core data and logs from the pilot holes and laterals. Comprehensive geomechanical and image log data integrated with the fiber-optic data across individual stages and clusters contributed to an improved understanding of the effect of stage spacing and cluster density practices across the heterogeneous unconventional reservoirs such as the Marcellus. The results significantly improved stimulation effectiveness and optimized recovery efficiency. The microseismic and fiber-optic data obtained during the hydraulic fracture simulations and subsequent DTS data acquired during production served as constraining parameters to evaluate stage and cluster efficiency on the MIP-3H and MIP-5H wells. Deformation effects related to preexisting fractures and small faults are a significant component to improve understanding of completion quality differences between stages and clusters. The distribution of this deformation and cross-flow between stages as shown by the DAS and DTS fiber-optic data during stimulation demonstrates the differences in completion efficiency among stages. The initial and evolving production efficiency over the last several years of various stages is illustrated through ongoing processing of continuous DTS. Reservoir simulation and history matching the well production data confirmed the subsurface production response to the hydraulic fractures. Engineered stages that incorporate the distribution of fracture swarms and geomechanical properties had better completion and more importantly production efficiencies. We are working to improve the modeling to understand movement within individual fracture swarms and history match at the individual

stage. As part of an additional MSEEL well pad underway incorporates advanced and cost-effective technology that can provide the necessary data to improve engineering of stage and cluster design, pumping treatments and optimum spacing between laterals, and imaging of the stimulated reservoir volume in the Marcellus and other shale reservoirs.

Introduction

The multidisciplinary and multi-institutional MSEEL team worked on geoscience, engineering, and environmental research in collaboration with Northeast Natural Energy LLC., several industrial partners, and the National Energy Technology Laboratory of the US Department of Energy. The objective of the Marcellus Shale Energy and Environment Laboratory (MSEEL) is to provide a long-term collaborative field site to develop and validate new knowledge and technology to improve recovery efficiency and minimize environmental implications of unconventional resource development. MSEEL began on the fall of 2015 with the drilling across from the City of Morgantown, West Virginia of the Northeast Natural Energy MIP-3H and MIP-5H and the vertical MIP-SW scientific and microseismic observation well. The site incorporates data from MIP-4H and MIP-6H wells, previously drilled in 2011. Logs were run on the lateral of the MIP-3H, and the MIP-3H was instrumented with a permanent fiber-optic cable (Figure 1). A cored vertical pilot bore-hole, a microseismic observation well, and surface geophysical and environmental monitoring stations completed the site. We have reported on numerous environmental observations, which show that the drilling, completion and production of the wells has had minimal environmental impact (e.g., Hakala et al. 2017; Sharma et al. 2017; Ziemkiewicz, 2017). The MIP production wells at the MSEEL site can easily supply the entire gas demand of the city. This paper will concentrate on the comprehensive geomechanical and image log data on the MIP-3H and integration with the fiber-optic data across individual stages and clusters. The results contributed to an improved understanding of the effect of stage spacing and cluster density practices across the heterogeneous unconventional shale reservoirs such as the Marcellus, and significantly improved stimulation effectiveness and optimized recovery efficiency.

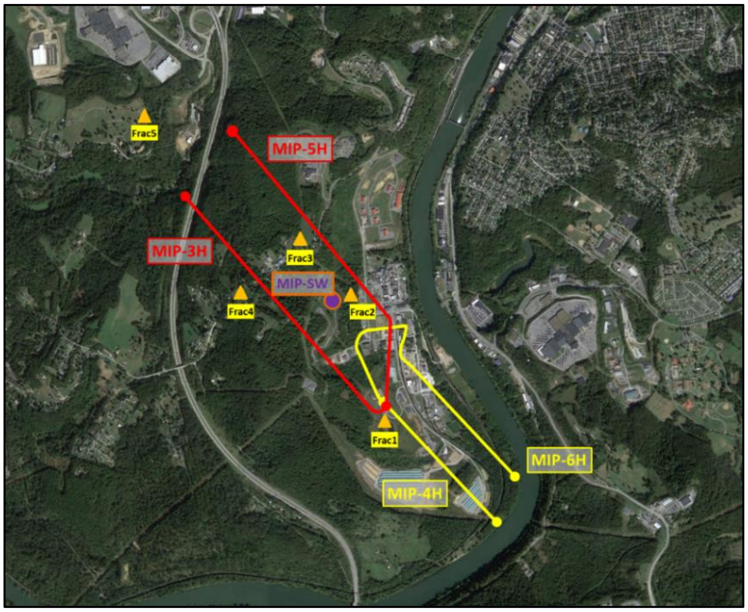

Figure 1. The Marcellus Shale Energy and Environment Laboratory (MSEE) is located across the Monongalia River from Morgantown, West Virginia. The MSEEL site consists of four horizontal production wells (MIP), one scientific/microseismic observation well (purple dot), and five surface seismic stations (yellow triangles).

Methods/Procedures

As part of the MSEEL project two new horizontal wells MIP-3H and MIP-5H were completed in 2015. Fiber optics technology including distributed acoustic sensing (DAS) and distributed temperature sensing (DTS) were deployed in the MIP-3H horizontal well to provide continuous subsurface vibration and temperature sampling during stimulation. The entire lateral of the MIP-3H was logged with a comprehensive suite of logs including geomechanical and image logs. The MIP-3H stimulation over 28 stages involved injection, at high pressure, averaging 8500 psi (58.6 MPa), to break the formation and establish a complex network of permeable fracture pathways. Microseismic data was recorded at the MIP-SW well located between the MIP-3H and MIP-5H (Figure 1). Microseismic events were numerous and displayed a consistent N59^{o}E orientation (Figure 2) (Wilson et al. 2018). The microseismic events showed wide vertical variation between stages with most events located in the units well above the landing zone in the lower Marcellus Shale (Figure 2). Logging of the MIP-3H lateral indicated several small faults and more than 1,600 fractures healed with calcite cement (Carr et al. 2017). Most fractures observed in the lateral were oriented N85^{o}E. Natural fractures provide planes of weakness that can play a significant role in production performance of shale wells by capturing induced fractures during stimulation and contributing to a complex fracture network during hydraulic fracturing.

The extremely large and diverse (multiple terabyte) datasets required a custom software system for analysis and display of fiber-optic DAS and DTS data and subsequent integration with microseismic data, core data and logs from the pilot holes and laterals. As an example, stage 10 contained over 150 fractures and several faults. Comprehensive geomechanical and image log data integrated with the fiber-optic data across individual stages and clusters contributed to an improved understanding of the effect of stage spacing and cluster density practices across the heterogeneous unconventional reservoirs such as the Marcellus.

Results

Among other attributes, temperature, energy and instantaneous frequency were calculated for several stimulated stages in MIP-3H lateral. One common way to visualize the DTS and DAS data is to use a waterfall plot with the measured depth of the well on the vertical axis and number of the timesteps in the horizontal axis. The color shows the calculated temperature or energy attribute for that timestep. The MIP-3H stimulation over 28 stages involved injection, at high pressure, averaging 8500 psi (58.6 MPa), to break the formation and establish a complex network of permeable fracture pathways Stage 10 shows the stimulation (Figure 3c), and the expected cooling of stage 10 as large quantities of surface-temperature water are injected into the reservoir with a temperature approaching 170^{o}F. The plug-and-perf mechanism is employed for the completion of the MIP-3H. This procedure seals the direct connection between Stage 10 and Stage 9 through the wellbore, and leakage around the plug or through cemented annulus as cooling in the previous Stage 9 was not observed (Figure 3a). Stage 10 DAS amplitude shows and uneven stimulation with energy concentrated in clusters 1, 2 and 5 (Figure 3b). The energy plot does not reveal detectable energy for Stage 9 (Figure 3b). However, expanding the scale of the DTS waterfall plot to encompass warming shows warming of Stage 9 during stimulation of Stage 10 (Figure 4a). Amini et al., 2017 and Carr et al., 2017 noticed this temperature rise for several other stages in MIP-3H. They suggested that numerous fractures and fault close to the stage boundaries are possibly responsible for this abnormal observation. Ghahfarokhi et al., 2019 showed evidence for long-period long-duration seismic events resulted from fault and fractures re-activation. Stimulation of the Stage 9 took place around 2 hours before Stage 10 stimulation. The fracturing fluid of Stage 9 rested at the formation and got warmed and approached reservoir temperature. Subsequent stimulation of Stage 10 pushed the warmed fluid of stage 9 back toward the well through fractures and faults. High fracture intensity close to the base of the Stage 10 and top of the Stage 9 were observed in wireline image logs (Carr et al. 2017).

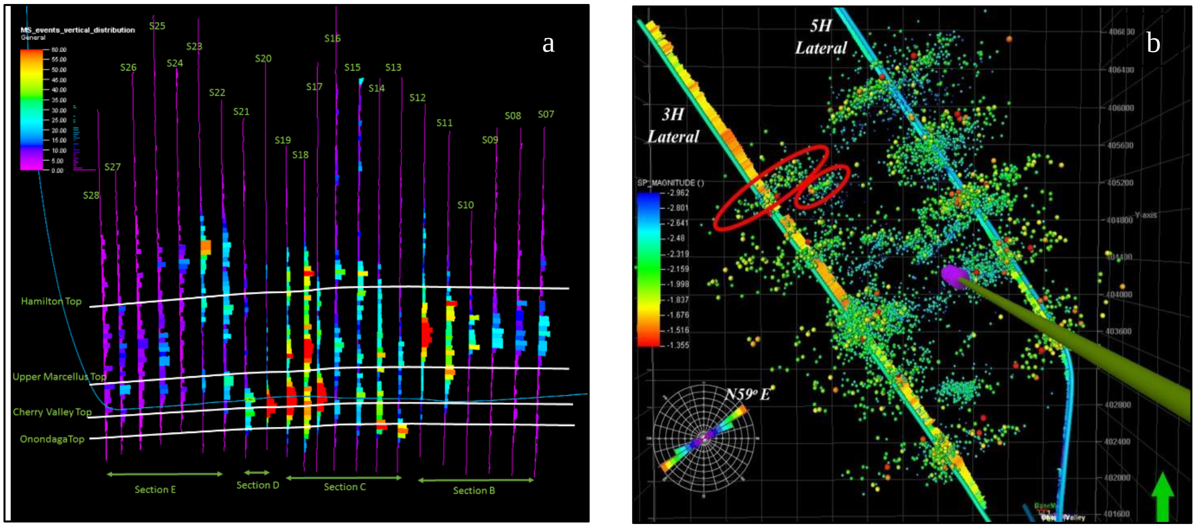

Figure 2. (a) The vertical distribution of microseismic events varies significantly along the MIP-3H lateral and is concentrated significantly above the landing zone in the lower Marcellus Shale. (b) The orientation of microseismic events in both the MIP-3H and MIP-5H is consistently N59ºE and like other wells in north-central West Virginia and southwest Pennsylvania. Image (b) modified from Wilson et al., 2018.

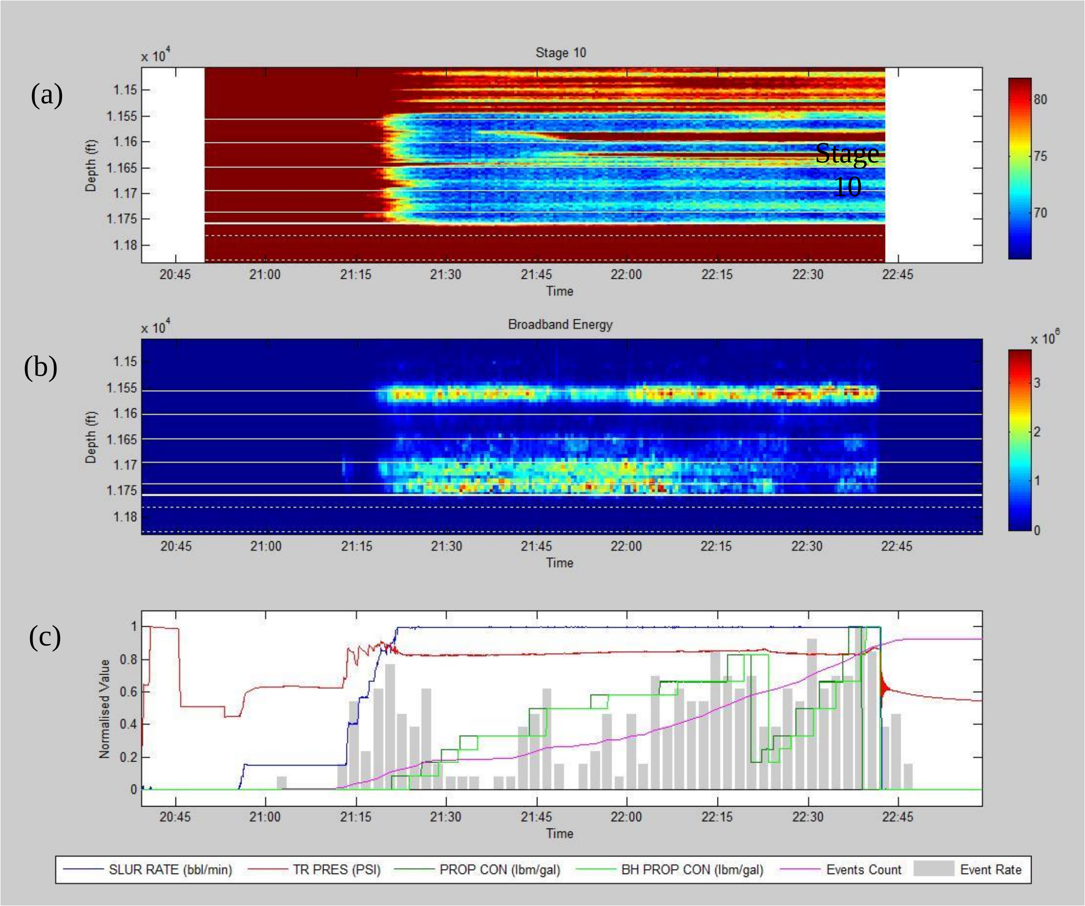

Figure 3. (a) Waterfall plot of distributed temperature sensing (DTS) data for Stage 10 and part of the previous Stage 9 and a portion of the lateral toward the heel showing the significant cooling of Stage 10 as large quantities of fracture fluid and proppant at near surface temperature are injected in the Marcellus Shale reservoir. (b) Waterfall plot of distributed acoustic sensing data (DAS) as broadband energy for Stage 10 and part of the previous Stage 9 showing the uneven distribution with energy concentrated in clusters 1, 2 and 5. Clusters 3 and 4 appear to be unstimulated. (c) Pumping scheduled for Stage 10 plotted on the same time scale as the DTS and DAS waterfall plots. Image modified from Kavousi Ghahfarokhi et al., 2018.

Kavousi Ghahfarokhi and others (2018) applied several common seismic attributes to the DAS data. These attributes in addition to energy include instantaneous attributes, and dominant frequency. The computations were undertaken through custom processing software developed in the MSEEL research group at West Virginia University. Low frequency zone identified in instantaneous frequency attribute was observed in Stage 9 (Figure 4b). This was attributed to presence of fluid that transferred cross-stage during hydraulic fracturing, and the frequency damping of the vibrations around the fiber (Kavousi Ghahfarokhi et al., 2018).

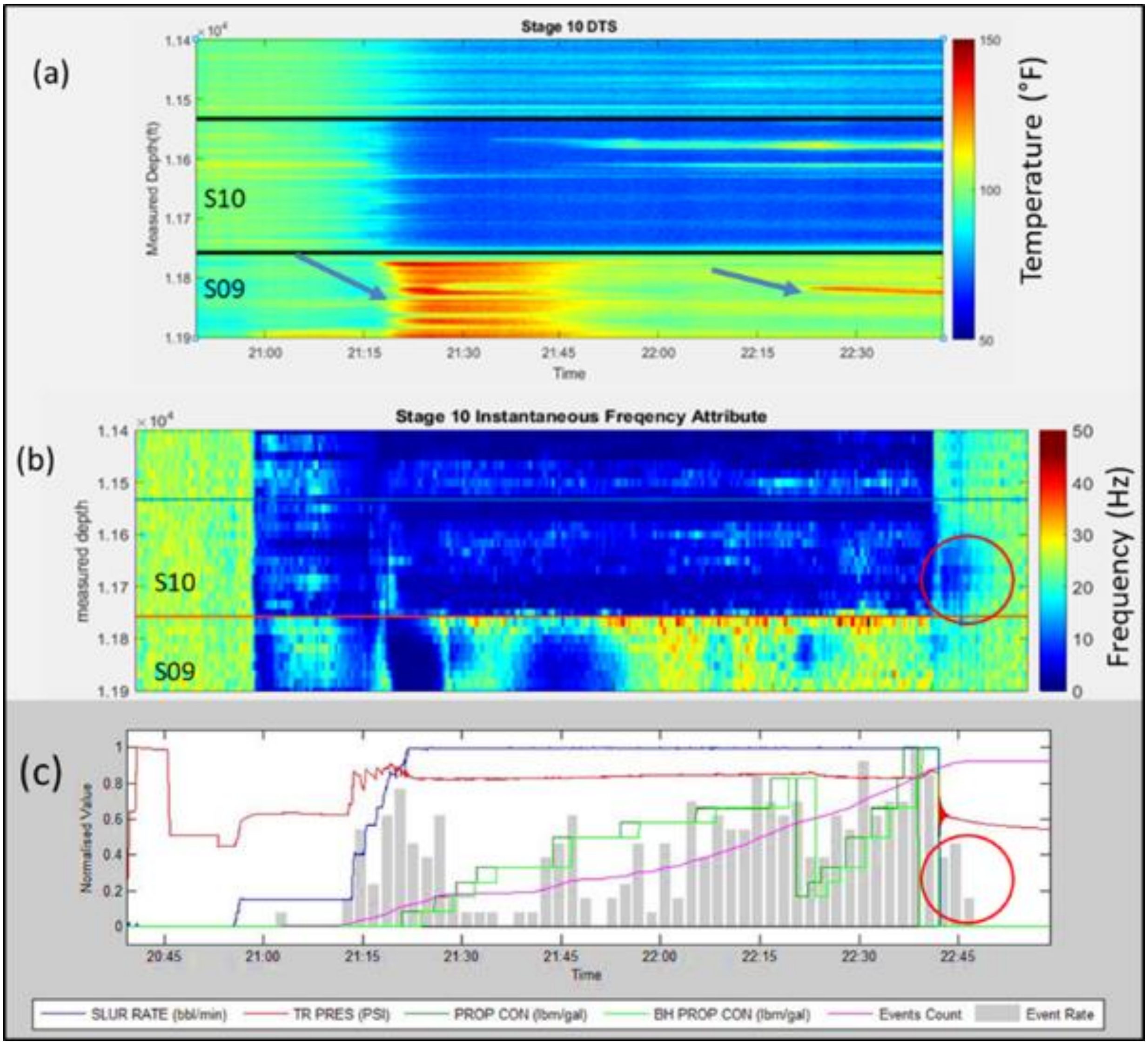

Figure 4. (a) Waterfall plot of distributed temperature sensing (DTS) data for Stage 10 and part of the previous Stage 9 and a portion of the lateral toward the heel showing the significant cooling of Stage 10 as large quantities of fracture fluid and proppant at near surface temperature are injected in the Marcellus Shale reservoir. Scale has been expanded from Figure 3a. Note warming observed in Stage 9 during stimulation of Stage 10. (b) Plot of instantaneous frequency. Low frequency zones are observed when there is a temperature rise in Stage 9. Note that the decreased injection of proppant also creates low frequency zones in Stage 9. Clusters 3 and 4 appear to be unstimulated. (c) Pumping scheduled for Stage 10 plotted on the same time scale as the DTS and DAS waterfall plots. Image modified from Kavousi Ghahfarokhi et al., 2018.

Discussion

A conceptual model was proposed as an attempt to explain the effect of the numerous preexisting N85°E healed fractures and faults observed in logs with observations during fracture stimulation in the MIP-3H (Figure 5). These observations during fracture stimulation include: clusters of microseismic events centered well above the lateral and orientated N59°E, and the observed significant warming as measured by DTS and attributes as computed from DAS such as instantaneous frequency in previous stages associated with fractures in the lateral. The rapid injection during fracture stimulation of an average of 255 cubic feet of proppant and fluid for every foot of the 6,058 feet (1846m) completed lateral would rapidly change both pore pressure, and vertical and lateral stresses. With the N36°W orientation of the MIP-3H lateral (Figure 1), fracturing and injection could occur along non-critically oriented N79°E preexisting fractures in the lower Marcellus Shale and predominately expessed in the aseismic "slow slip" with low frequency seismic events that are not picked up by standard microseismic monitoring. Such low frequency events have been observed in surface seismometers, downhole geophones and DAS data during stimulation of Stage 10 (Ghahfarokhi et al., 2019). The oblique orientation of the lateral to prexisting fractures could explain the warming as detected by DTS of previous stages to near formation temperatures by movement of fluids previously injected and warmed by the formation through stimulated fractures communicating from one stage to the previous stage(s). This change in temperature in the previous stage(s) appears to be more prevalent between stages with numerous observed faults and fractures. Microseismic events are centered significantly above the stimulated interval and follow optimal oriented fractures to the present day stress regime. The observed microseismic events may not be a direct expression of stimulated fractures and propopant placement in the targeted lower Marcellus shale, but indirect expression in the overlying stratigraphic units imposed by the injection of more than 250 cubic feet of sand and fluid per foot of lateral.

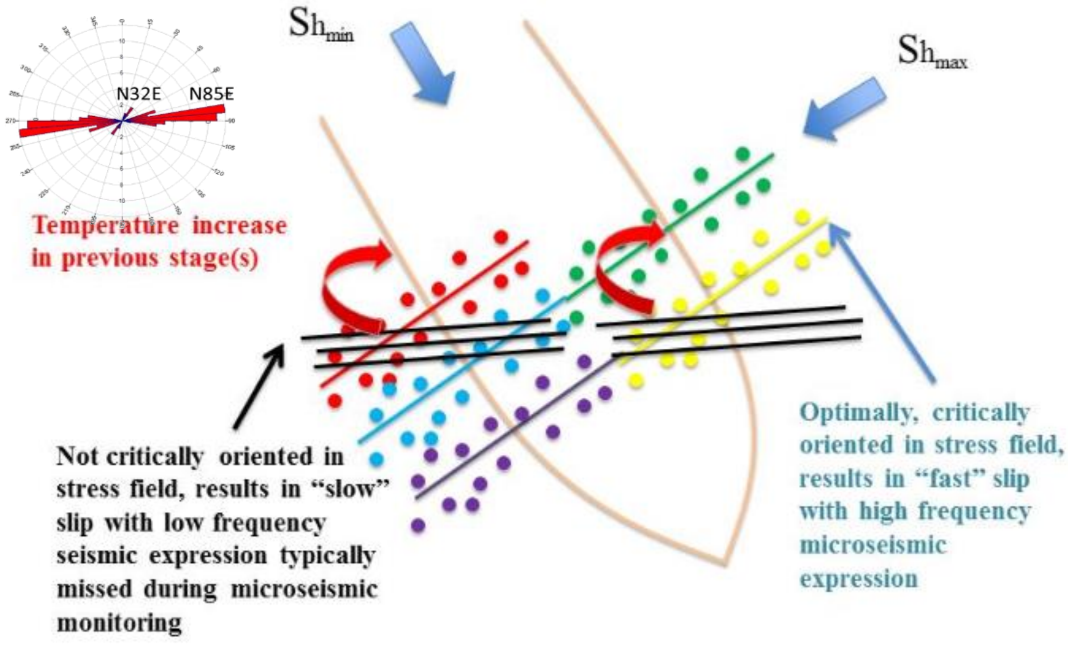

Figure 5. Conceptual model of observed pattern of the numerous preexisting N85°E fractures and faults observed in logs and plotted on the Rose diagram, microseismic orientated N59°E, warming observed in DTS in previous stages during fracture stimulation in the MIP-3H. Basic figure was modified from Das and Zoback, 2012. Movement and injection along non-critically oriented preexisting fractures in the lower Marcellus Shale resulted in the "slow" slip with low frequency seismic expression that was not picked up by microseismic monitoring and movement of fluids warmed by the formation to previous stimulated stages. Microseismic events follow optimal oriented fractures to the present-day stress regime and are centered significantly above the stimulated interval. The observed microseismic events may be the expression of the stress on overlying layers imposed by the injection of more than 250 cubic feet of sand and fluid per foot of lateral.

Stages 13 through 19 were designed using geomechanical properties from the logs along the lateral. Comparing the geomechanical moduli and properties between the geometric stage 10 and one of the engineered stages such as Stage 14 shows the wide scatter of geomechanical moduli and properties in stage 10 and the tighter cluster in Stage 14 (Figure 6). Stage 14 shows a more even fracture stimulation. DTS dated collected since early 2016 to the present and processed with MSEEL software illustrates temperature variations for each stage relative to daily average temperature of each stage along the well (Figure 7) (Carr et al. 2018). On the production de-trended DTS attribute, general cooling from the heel to the toe is observable, but some geometric stages such as 10 and 11 and 20-21 and 23-28 are relatively warmer. Also standing out are the cooler engineered stages 17-19. Based on the processed DTS data, the non-optimum stimulation of Stage 10 appears to have resulted in apparent non-optimum production (Carr et al. 2007; Amini et al. 2007 and Ghahfarokhi et al. 2018). Using production logs and DTS data production in engineered stages 13 through 19 appear to have on average increased production 20 percent compared to the geometric completion techniques (Figure 8).

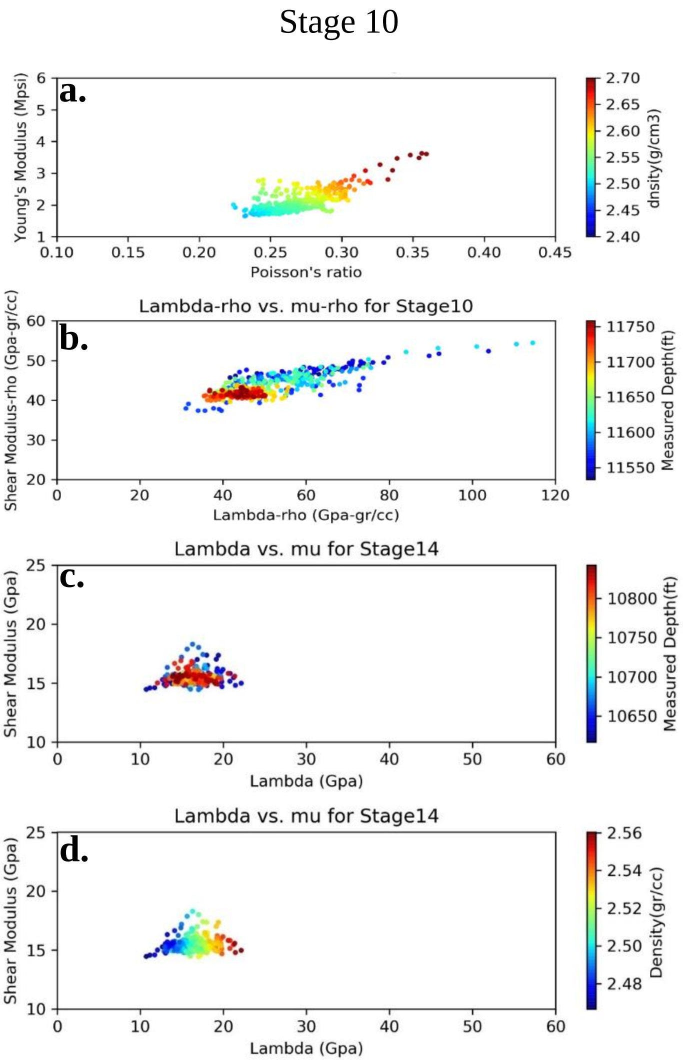

Figure 6. (a) Poisson's Ratio versus Young's Modulus for geometric Stage 10 attributed with density showing the scatter. Density for higher values approach calcite (2.71 gm/cc). (b) Lambda-rho versus mu-rho plot for geometric Stage 10 attributed with depth along the stage. (c) Lambda versus mu for engineered Stage 14 attributed with depth along the stage. (d) Lambda versus mu for engineered Stage 14 attributed with density along the stage. The engineered Stage 14 shows a tighter distribution of geomechanical properties, which is believed to have resulted in higher stimulation efficiency than geometric Stage 10.

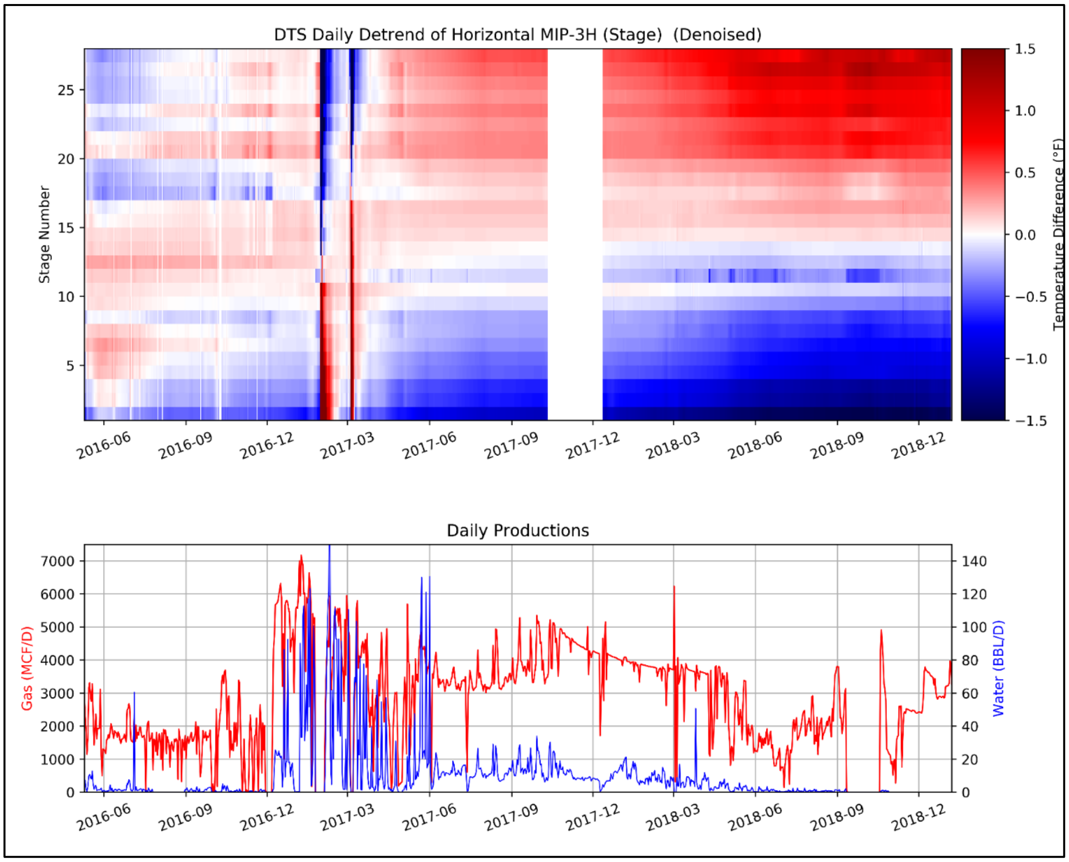

Figure 7. The de-trended DTS attribute is averaged to the stage scale. The vertical lines show the time that MIP-3H was cleaned out with water and then with nitrogen foam prior to production logging. Geometric Stage 10 shows a higher temperature that is attributed to lower gas production. Modified and updated from Carr et al. 2018.

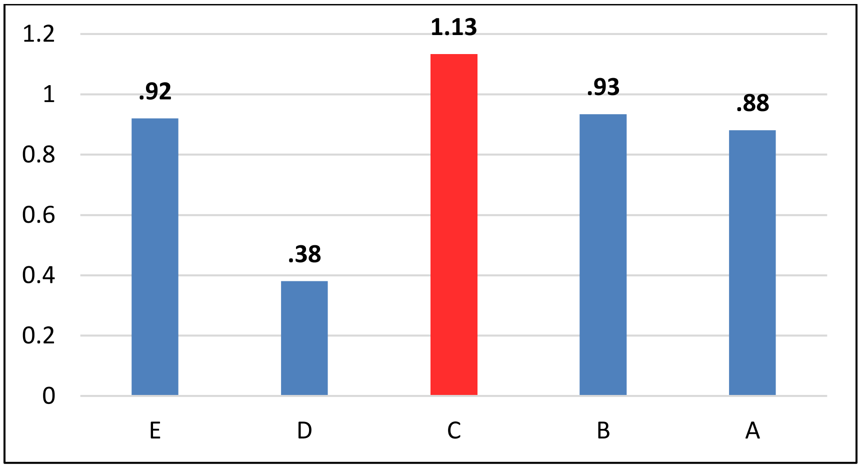

Figure 8. MIP 3H gas production (mcf/ft) showing that the engineered design for stages 13 through 19 represented by C using data obtained during production logging of the MIP-3H. Engineered stages in section C have approximately 20% increased production compared to standard geometric completion techniques. EUR for future wells could be 10-20% greater if one can exploit the technologic advantages gained through MSEEL in a more cost-effective fashion

Conclusions

An improved understanding of stimulation efficiency is obtained from integration of the extremely large and diverse (multiple terabyte) datasets using a custom software system for analysis and display of fiber-optic distributed acoustic sensing (DAS) and distributed temperature sensing (DTS) data integrated with completion observation, microseismic data, core data and logs from the pilot holes and laterals. Comprehensive geomechanical and image log data along with processed DAS and DTS data across individual stages and clusters contributed to an improved understanding of the effect of stage spacing and cluster density practices across the heterogeneous unconventional reservoirs such as the Marcellus Shale. The results significantly improved stimulation effectiveness and appears to have improved recovery efficiency.

Microseismic and fiber-optic data obtained during the hydraulic fracture simulations and subsequent DTS data acquired during production serves as constraining parameters to evaluate stage and cluster efficiency on the MIP-3H well. Deformation effects and complexity related to preexisting fractures and small faults are a significant component of completion quality differences between stages and clusters. DAS and DTS fiber-optic show the effect of this deformation and cross-flow between stages during stimulation and demonstrates the differences in completion efficiency among stages.

Ongoing processing of continuous DTS illustrates initial and evolving production efficiency over the last several years of various stages. Reservoir simulation and history matching the well production data confirmed the subsurface production response to the hydraulic fractures. Engineered stages that incorporate the distribution of fracture swarms and geomechanical properties had better completion and more importantly production efficiencies. We are working to improve the modeling to understand movement within individual fracture swarms and history match at the individual stage.

As part of ongoing work with DTS and DAS monitoring at the MIP-3H and an additional MSEEL well pad underway we will incorporate next-generation cost-effective technology to determine feasibility of applying lessons learned on an “every well” basis to improve engineering of stage and cluster design, pumping treatments and optimum spacing between laterals, and imaging of the stimulated reservoir volume in the Marcellus and other shale reservoirs. MSEEL is working to evaluate and leverage this improved understanding gained to drill better wells by increasing gas recovery while minimizing wellbore risk and lower costs.

References

Carr, T.R., Wilson, T.H., Kavousi, P., Amini, S., Sharma, S., Hewitt, J., Costello, I., Carney, B.J., Jordon, E., Yates, M. and MacPhail, K. 2017. Insights from the Marcellus Shale Energy and Environment Laboratory (MSEEL). Unconventional Resources Technology Conference held in Austin, Texas, USA, 24-26 July 2017. 9p., https://doi.org/10.15530/URTEC-2017-2670437.

Carr, T. R., Kavousi Ghahfarokhi, P. Carney, BJ., Hewitt, J., and Vagnetti, R. 2018. A New Algorithm for Processing Distributed Temperature Sensing (DTS), Conference Proceedings Eastern Section Society Petroleum Engineers, Society Petroleum Engineers, 7-11 October, Pittsburgh, PA, SPE-194814-18ERM-MS, 16p. https://doi.org/10.2118/191814-18ERM-MS .

Hakala, J.A.; Crandall, D.; Moore, J.; Phan, T.; Sharma, S.; Lopano, C. Laboratory-scale studies on chemical reactions between fracturing fluid and shale core from the Marcellus Shale Energy and Environmental Laboratory (MSEEL) site. Unconventional Resources Technology Conference, Austin, TX, 24 – 26 July, https://doi.org/10.15530-urtec-2017-2670856.

Kavousi, P., Carr, T., Wilson, T., Amini, S., Wilson, C., Thomas, M., MacPhail, K., Crandall, D., Carney, B.J., Costello, I. and Hewitt, J. 2017. Correlating distributed acoustic sensing (DAS) to natural fracture intensity for the Marcellus Shale. In *SEG Technical Program Expanded Abstracts 2017* (pp. 5386-5390). Society of Exploration Geophysicists. https://doi.org/10.1190/segam2017-17675576.1

Kavousi Ghahfarokhi, P., Carr, T., Song, L., Shukla, P. and Piyush P. 2018. Seismic Attribute Application for the Distributed Acoustic Sensing Data for the Marcellus Shale: A New Insights to Cross-Stage Flow Communication. SPE Hydraulic Fracturing Technology Conference held in The Woodlands, TX, USA, 23-25 January 2018. https://doi.org/10.2117/189888-MS.

Kavousi Ghahfarokhi, P., Wilson, T.H., Carr, T.R., Kumar, A., Hammack, R. and Di, H., 2019. Integrating distributed acoustic sensing, borehole 3C geophone array, and surface seismic array data to identify long-period long-duration seismic events during stimulation of a Marcellus Shale gas reservoir. Interpretation, *7*(1), pp. SA1-SA10. https://doi.org/10.1190/INT-2018-0078.1.

Sharma S., Carr, T. R., Mouser, P. J., Wrighton, K., Cole, D., Wilkins, M., Darrah, T., and Hakala, A. 2017. Biogeochemical Characterization of Core, Fluids, and Gas at MSEEL Site. Unconventional Resources Technology Conference held in Austin, Texas, USA, 24-26 July 2017. 8p. https://doi.org/10.15530/urtec-2017-2669965.

Wilson, T. H., Carr, T., Carney, BJ., Yates, M., MacPhail, K., Morales, A., Costello, I., Hewitt, J., Jordon, E., Uschner, N., Thomas, M., Akin, S., Oluwaseun, M., Asbjoern J., Hogarth, L., Anifowoshe, O., and Naseem, K. 2018. Marcellus Shale model stimulation tests and microseismic response yield insights into mechanical properties and the reservoir DFN. Interpretation, 6(2), T231-T243. Volume 6, Issue 2 (May 2018), Society Exploration Geophysicists. https://doi.org/10.1190/int-2016-0199.1.

Ziemkiewicz, P.F. 2017. The Marcellus Shale Energy and Environmental Laboratory (MSEEL): Water and Solid Waste Findings--Year One. Unconventional Resources Technology Conference held in Austin, Texas, USA, 24-26 July 2017. 9p. https://doi.org/10.15530/urtec-2017-2669914.